Available at www.sciencedirect.com

ScienceDirect

journal homepage: www.elsevier.com/locate/he

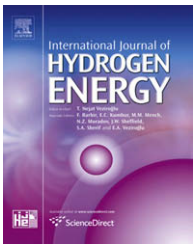

Fabrication of Ni nanowires for hydrogen evolution reaction in a neutral electrolyte

Po-Chun Chen, Yun-Min Chang, Pu-Wei Wu, Yu-Fan Chiu*

Department of Materials Science and Engineering, National Chiao Tung University, 1001 University Road, Hsin-Chu 300, Taiwan, ROC

ARTICLE INFO

Article history:
Received 23 February 2009
Received in revised form
17 May 2009
Accepted 29 May 2009
Available online 23 June 2009

Keywords:
Ni nanowires
Hydrogen evolution reaction
Neutral electrolyte
Template synthesis

ABSTRACT

Hydrogen evolution reaction in 1 M Na_2SO_4 was investigated using Ni nanowires in diameter of 250 nm with exposed lengths of 20, 35, and 45 μm, respectively. The Ni nanowires were fabricated by a direct-current pulse electrodeposition technique using an anodic aluminum oxide template, followed by selective removal of the supporting pore walls. Scanning Electron Microscope images revealed structural stabilities and X-ray diffraction pattern indicated a polycrystalline fcc phase. In current–potential (*i–V*) polarizations, the Ni nanowires with longer exposed lengths demonstrated larger current responses. Analysis from impedance spectroscopy confirmed increasing double-layer capacitances with longer Ni nanowires. In galvanostatic lifetime experiments, the free-standing Ni nanowires exhibited a reduced overpotential over that of supported ones. Similar procedures were performed for the oxygen evolution reaction in both *i–V* and lifetime measurements. For the Ni nanowires of 45 μm length, we estimated the energy cost for hydrogen production was 5.24×10^5 J/mole.

1. Introduction

Hydrogen is a promising energy carrier because its oxidation with oxygen in fuel cells provides electricity without harmful CO_2 emissions [1]. Among many hydrogen production schemes explored, water electrolysis is considered as the simplest [2–4]. The water electrolysis involves an electrochemical reaction to decompose water under sufficient voltage drive. Unfortunately, large-scale implementation using the water electrolysis to produce hydrogen is hindered by severe polarization loss. To reduce overpotentials for the hydrogen evolution reaction (HER), a variety of electrocatalysts has been explored [5–8]. However, for low-cost industrial applications, the Ni and its alloys are recognized as potential electrode materials [9–11].

Electrolytes in alkaline (KOH) or acidic (H_2SO_4) solutions are often used in HER studies [12–14]. On the other hand, the neutral solution has received less attention [15–17]. In principle, HER occurring in a neutral electrolyte suffers from slower kinetics as compared to that of alkaline one because of larger ohmic loss. Nevertheless, selection of neutral electrolyte is necessary for systems that are unstable in alkaline or acidic environments. For example, a possible application is to construct a miniaturized water electrolyzer for Micro Electro Mechanical Systems-based (MEMS) devices. It is because MEMS are typically built upon Si platforms, which are susceptible to corrosion in alkaline solutions.

Nanostructured materials prepared from template synthesis approaches have attracted considerable attention recently for their prospects in fabricating devices for magnetic, electronic, and electrochemical applications [18–20]. A popular template to date is the anodic aluminum oxide (AAO). The AAO consists of perpendicularly aligned pore channels with adjustable diameters and densities. Earlier work by Li et al. and Sapp et al. concerned growths of nanomaterials within the pore channels for high-rated lithium batteries and thermoelectrical materials

* *Corresponding author*. Tel.: +886 3 5131227; fax: +886 3 5724727.
E-mail address: ppwu@mail.nctu.edu.tw (P.-W. Wu).

0360-3199/$ – see front matter © 2009 International Association for Hydrogen Energy. Published by Elsevier Ltd. All rights reserved.
doi:10.1016/j.ijhydene.2009.05.126

[21,22]. It is recognized that electrode structures with excessive surface areas can be constructed in this way to reduce undesirable polarization loss.

In this work, we fabricated Ni nanowires by a direct-current (dc) pulse electrodeposition technique using the AAO as a template. We designed the Ni nanowires with supported and unsupported AAO pore walls to expose various surface areas. Electrochemical analysis was conducted to identify the optimized HER performance.

2. Experimental

AAO templates (25 mm in diameter) with an average pore diameter of 250 nm in thickness of 60 μm were purchased from Whatman International Ltd. Their pore density and wall thickness were $8.0 \times 10^8/cm^2$ and 100 nm, respectively. First, the AAO template was sputtered with a thin metal film of 200 nm (Pt or Au) serving as the conductive substrate. A dc pulse electrodeposition method with the on–off mode (1:1 in s) and current density of 28 mA/cm^2 was employed to grow Ni nanowires. The plating electrolyte contained 120 g/L of $NiSO_4 \cdot 6H_2O$, 60 g/L of $NiCl_2$, 30 g/L of H_3BO_3, and 2 g/L of polyethylene glycol (Mw. 2000). The bath temperature was kept at 25 °C at pH of 4.

The dc pulse electrodeposition lasted 60 min to obtain Ni nanowires of 45 μm embedded within the 60 μm-deep AAO pore channels. This corresponded to an aspect ratio of 180 for the as-prepared Ni nanowires. Subsequently, the sample was immersed in a 0.5 M KOH solution, followed by washing in deionized water. The purpose for the KOH treatment was to remove the AAO pore walls, leaving Ni nanowires with exposed lengths between 20 and 45 μm. Accordingly, the height of the supporting AAO wall at the base of the Ni nanowires became 25–0 μm. The exposed length of 45 μm was essentially the height for the free-standing Ni nanowires. In this way, we were able to explore the distinction of supported and unsupported Ni nanowires in HER behaviors.

In electrochemical analysis, an aqueous solution of 1 M Na_2SO_4 was used. A three-electrode configuration was adopted where the reference electrode was a Ag/AgCl electrode with saturated KCl, and the counter electrode was a Pt foil (6.25 cm^2). The Ni nanowires with a geometric area of 1 cm^2 were fastened by a Teflon holder serving as the working electrode. Electrochemical measurements in current–potential polarizations (*i*–*V*) were conducted by a Solartron SI 1287 with a scan rate of 5 mV/s for −0.2 to −1.6 V. In addition, a planar Ni plate (99.9 wt%) was evaluated for comparison purpose. We also performed the *i*–*V* measurements for −0.2 to 1.8 V for the oxygen evolution reaction (OER). Galvanostatic responses were recorded at 30 mA/cm^2 to determine lifetime performance for both HER and OER in order to estimate the energy cost for hydrogen production. Impedance spectra were obtained at open circuit voltage with a stimulus of 10 mV for the frequency range of 1–10 kHz using a Solartron SI 1255B. Approximation fitting to the impedance curves was conducted by ZView software for the entire frequency range. All the electrochemical analysis was carried out at 25 °C.

Field-emission Scanning Electron Microscope (FE-SEM; JEOL-JSM-6700F) was used to observe the morphologies for the Ni nanowires. X-ray diffraction (XRD) was conducted by Siemens D5000 with a Kα of 1.54 Å to identify relevant phase present. Energy dispersive X-ray (EDX) analysis was adopted to analyze the composition for the Ni nanowires.

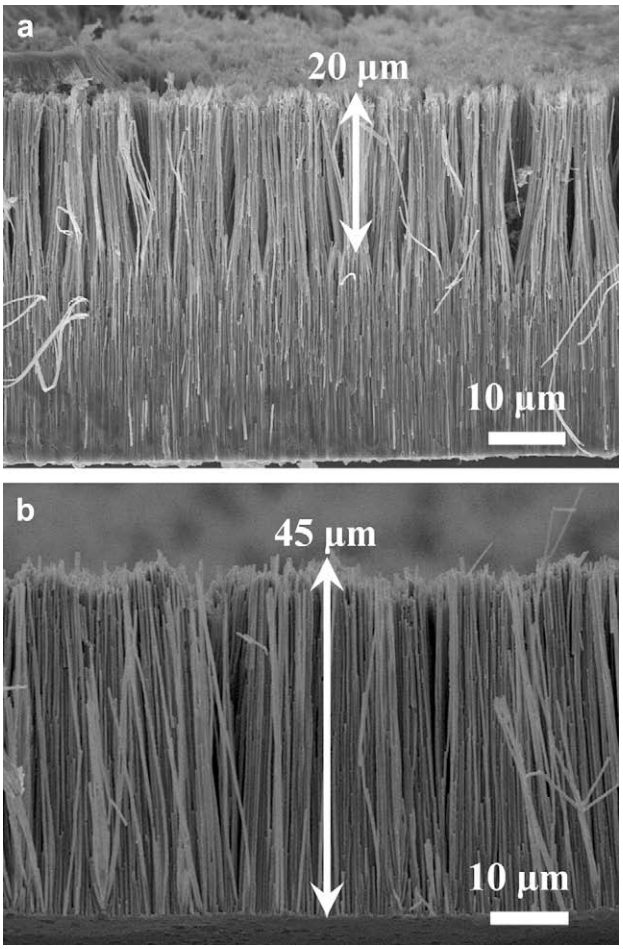

Fig. 1 – Cross-sectional SEM images for the Ni nanowires in exposed length of (a) 20 and (b) 45 μm, respectively.

3. Results and discussion

3.1. *Characterization of Ni nanowires*

The dc pulse electrodeposition is recognized as an effective method to deposit materials into pores of high aspect ratios. It is because the off-time in the depositing sequence allows redistribution of working ions to facilitate growths during subsequent on-time. After extensive tries, we were able to obtain the Ni nanowires without undesirable overplating at pore openings. After deposition for 60 min, the Ni nanowires with an average height of 45 μm were formed within the pore channels of the AAO template.

Fig. 1(a) and (b) present the cross-sectional SEM images of the Ni nanowires with the exposed lengths of 20 and 45 μm, respectively. As clearly shown, the Ni nanowires were aligned perpendicularly with impressive mechanical strengths. In

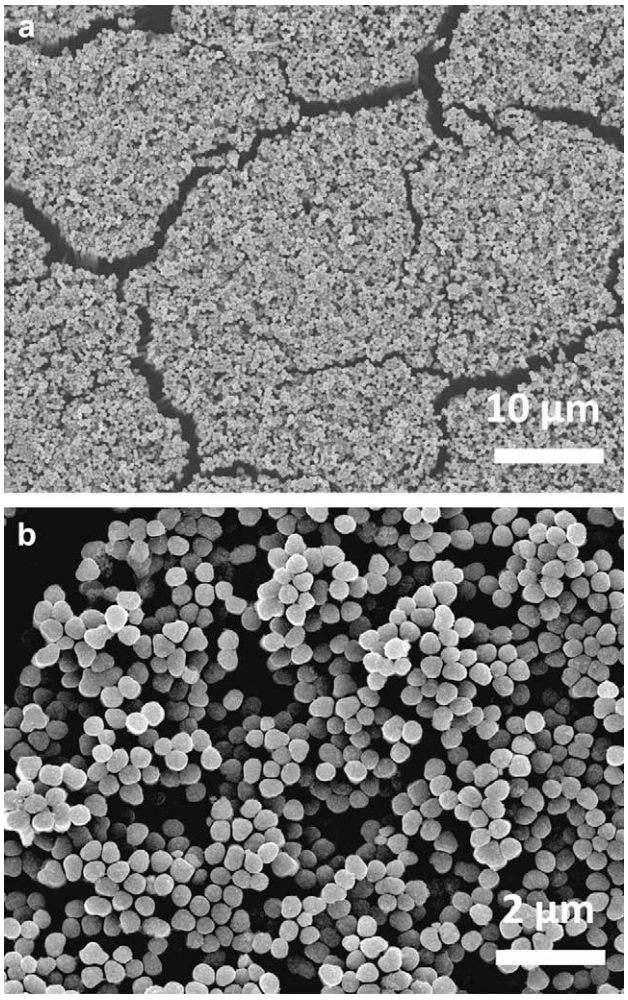

Fig. 2 – SEM images for the 45 μm Ni nanowires in top view for (a) low and (b) high magnification, respectively.

addition, their height was rather consistent, indicating the growth of Ni nanowires was taking place uniformly among individual pore channels. The diameter for the nanowires was estimated at 250 nm, which agreed with the pore diameter of the AAO template. It can be seen that partial removal of the AAO pore walls produced a negligible effect on the Ni nanowires, leaving them essentially intact. Furthermore, complete removal of the AAO template produced free-standing Ni nanowires without noticeable structural collapse. Analysis from EDX on the top portion of Fig. 1(a) confirmed the presence of Ni while mixtures of Ni and Al were identified at the bottom part.

Fig. 2(a) and (b) provide the SEM images in top view for the Ni nanowires without AAO supports in low and high magnifications, respectively. As shown, the Ni nanowires appeared in clusters with domain-like morphologies. In the high magnification image, the top portions of the Ni nanowires were touching each other slightly. At this stage, these free-standing Ni nanowires were anchored by the conducting layer at the bottom. We suspect that static charges among them are responsible for the observed bundle formations. The KOH etching rate in our case was estimated at 900 nm/min. This value is in line with what was reported earlier by Song et al. in a similar 3 M NaOH etching solution [23].

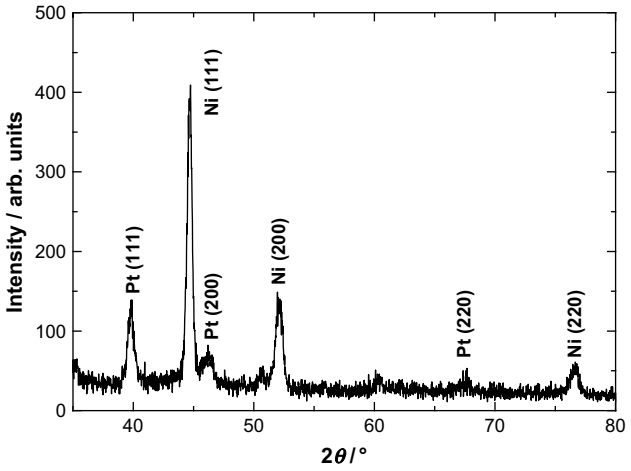

Fig. 3 – XRD pattern for the 45 μm Ni nanowires.

XRD pattern for the Ni nanowires after complete removal of the AAO template is exhibited in Fig. 3. The diffraction pattern revealed signals from those of Pt and Ni. The strongest one from the Ni nanowires was recorded at 44.74°, which was identified as the (111) plane. This agreed with a typical bulk polycrystalline fcc Ni where the highest peak is expected to appear at 44.50° for the identical plane (JCPDS 7440-02-0). In addition, relative intensities for those Ni diffraction peaks were in correct order as expected.

3.2. *Electrochemical analysis*

Fig. 4 demonstrates the i–V curves for the Ni nanowires with exposed lengths of 20, 35, and 45 μm, respectively. The planar Ni plate is also provided as the reference. In the neutral electrolyte, the equilibrium potential for the Ni nanowires was −0.2 V (vs. Ag/AgCl). Once cathodic overpotential was

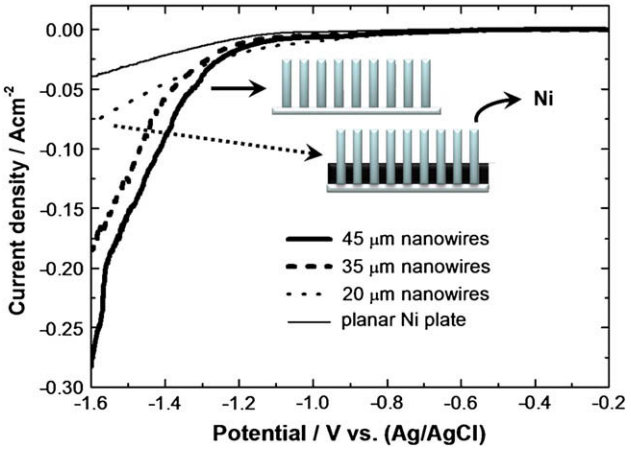

Fig. 4 – HER current–potential profiles for the Ni nanowires in exposed lengths of 20, 35, and 45 μm, as well as planar Ni plate.

Table 1 – Values for apparent and effective current densities for the Ni nanowires and planar Ni plate at selective potentials.

Sample	Surface area (cm^2)[a]	−1.20 V		−1.60 V	
		Apparent current (mA/cm^2)	Effective current (mA/cm^2)	Apparent current (mA/cm^2)	Effective current (mA/cm^2)
Planar Ni plate	1	4.16	4.160	39.39	39.390
20 μm nano-wires	126.1	16.44	0.130	78.94	0.626
35 μm nano-wires	220.3	27.00	0.123	186.28	0.846
45 μm nano-wires	283.1	30.20	0.108	282.23	0.997

a Based on geometric calculation from equation (1).

imposed, we started to record current responses. The current showed obvious increments when the potential reached −1.2 V. It can be seen that the Ni nanowires with longer exposed lengths exhibited larger current responses. This is likely since a longer exposed length for the Ni nanowires is equivalent to a larger surface area for the HER. In contrast, the planar Ni plate exhibited substantially reduced current values. Table 1 lists the apparent current densities at selected potentials of −1.2 and −1.6 V for the samples involved.

Since the *i*–*V* curves indicated that the Ni nanowires with longer exposed lengths exhibited improved electrocatalytic performances, a further discussion on the effective current densities for the HER is necessary. The actual surface area for the Ni nanowires could be estimated by the equation below;

$$A = \rho \times (\pi \times \gamma^2 + 2\pi\gamma \times t) \quad (1)$$

where *A* is the actual surface area, ρ is the number of the Ni nanowires in 1 cm^2 geometrical footprint, γ is the radius of the Ni nanowires, and *t* is the exposed length of the Ni nanowires. Careful SEM observations have determined the γ to be 125 nm. The ρ equaled to the pore density of the AAO template, which was $8.0 \times 10^8/cm^2$. This value agreed with earlier reports using identical AAO templates [24,25]. The values for actual surface area of the Ni nanowires, and their corresponding effective current densities are also provided in Table 1. Unexpectedly, the effective current densities for the Ni nanowires were substantially smaller than that of planar Ni plate. This suggests areas responsible for the HER in the Ni nanowires are rather limited. Due to the cluster formation in the Ni nanowires and an aspect ratio of 180, we believe that electrolyte transport to the bottom of the nanowires is hindered. It is because during HER, large amount of hydrogen bubbles were released and they would interfere with the electrolyte inflow. This behavior is expected to be particularly pronounced since the nanowire structures only allow vertical bubble escapes. Moreover, as pointed out by Kiuchi et al. and Cheng et al., the trapped gas bubbles contributed considerable ohmic

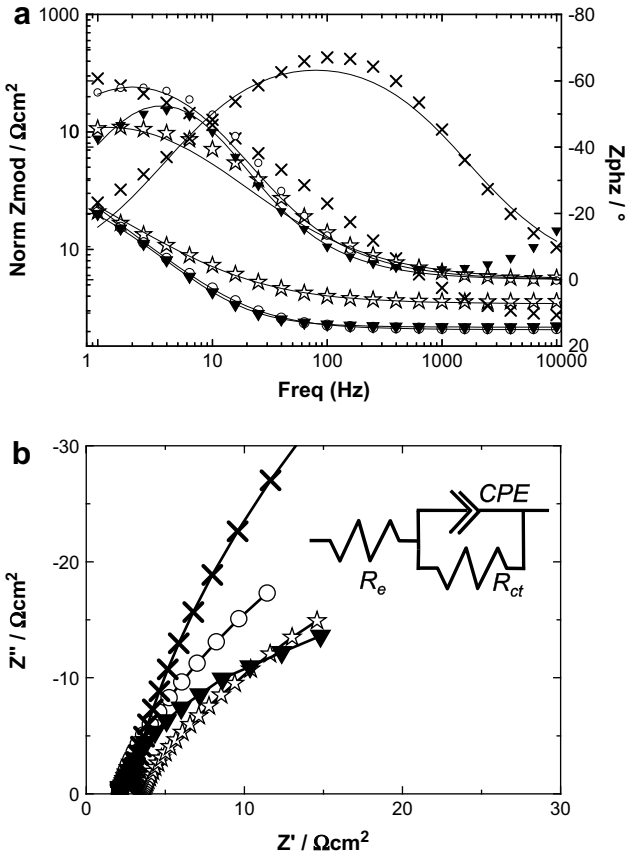

Fig. 5 – Impedance spectra in (a) Bode plot for the entire frequency range and (b) Nyquist plot for the high frequency regime for samples of planar Ni plate (×), and Ni nanowires in 20 (▼), 35 (○), and 45 (☆) μm, respectively.

resistance in the electrolyte that often resulted in loss of catalytic ability [26,27]. Therefore, we realize that the effective surface area for the HER was confined primarily at the top portion of the Ni nanowires. Similar results were recently reported by Kim et al. in their study of Ru nanorods for water electrolysis [28].

An alternative method to identify the electrochemical active surface area for the HER is determination of double-layer capacitance, which is typically acquired by impedance analysis at the open circuit voltage. It is because free from external overpotentials, the double-layer capacitance can be extracted without possible interference from redox pseudo-capacitance. Fig. 5(a) displays the Bode plots, and the associated simulation fitting from the entire frequency range for the supported and unsupported Ni nanowires, as well as planar Ni plate. The corresponding Nyquist plots in high frequency regime are also presented in Fig. 5(b). As shown, the impedance spectra revealed typical responses consisting of a distorted semicircle at high frequencies and Warburg impedance at low frequencies. Our impedance profiles appeared similar to what was reported recently by Michishita et al. in which the $La_{0.6}Sr_{0.4}CoO_3$ perovskite was studied in an alkaline electrolysis cell [29]. An equivalent circuit including constant phase element (CPE), electrolyte resistance (R_e), and charge transfer

Table 2 – Parameters from fitting impedance spectra obtained at the open circuit voltage for the Ni nanowires and planar Ni plate.

Sample	R_e (Ωcm^2)	R_{ct} (Ω/cm^2)	CPE-T (μF/cm^2)	CPE-P	Capacitance ($\mu F/cm^2$)
Planar Ni plate	2.40	307.00	249	0.81	42
20 μm nanowires	2.18	31.58	7950	0.88	2763
35 μm nanowires	2.07	88.57	9260	0.82	3925
45 μm nanowires	3.43	121.40	12290	0.68	4550

resistance (R_{ct}) was used to approximate the impedance profiles (shown in Fig. 5(b)). According to Vázquez-Gómez et al., at the open circuit voltage [30],

$$Z_{CPE} = \frac{1}{Q(j\omega)^{\alpha}} \tag{2}$$

where the values for α and Q could be estimated by a graphic approach proposed by Orazem et al. [31] as

$$\alpha = \frac{d\log[-Im(Z)]}{d\log(f)} \tag{3}$$

$$Q = \sin\left(\frac{\pi\alpha}{2}\right)\frac{-1}{Im(Z)\,(2\pi f)^{\alpha}} \tag{4}$$

The double-layer capacitance for the electrode can be derived by the following equation [32],

$$Q = C^{\alpha}\left(R_s^{-1} + R_{ct}^{-1}\right)^{1-\alpha} \tag{5}$$

Relevant parameters from the simulation fitting are listed in Table 2. It can be seen that the double-layer capacitance for planar Ni plate, and Ni nanowires of 20, 35, and 45 μm were 42, 2763, 3925, and 4550 $\mu F/cm^2$, respectively. Their ratio, taking the planar nickel plate as 1, turns out to be 1:66:93:108. This value is below 50% of what is listed in Table 1 from geometric estimations. Hence, we realize that substantial areas of the Ni nanowires are inaccessible to electrolyte contact. This effect is likely to become more pronounced when the HER is taking place. It is because once polarizations are imposed, the freshly produced gas bubbles would severely compromise electrolyte transport within the Ni nanowires. As a result, further reduction in the active surface area responsible for the HER is expected, and this explains the significant reduction in the effective current density for the Ni nanowires as opposed to that of planar Ni plate. Contributions from the Pt to the HER activity are negligible because the area of exposed Pt at the Ni nanowires bottom is finite. Besides, the limitation on electrolyte transport to the bottom further reduces possible Pt activity.

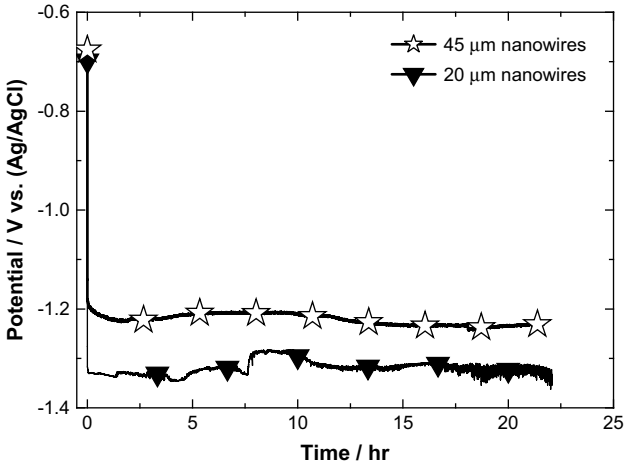

Fig. 6 – Galvanostatic HER profiles for the Ni nanowires in 20 (▼) and 45 (☆) μm, respectively.

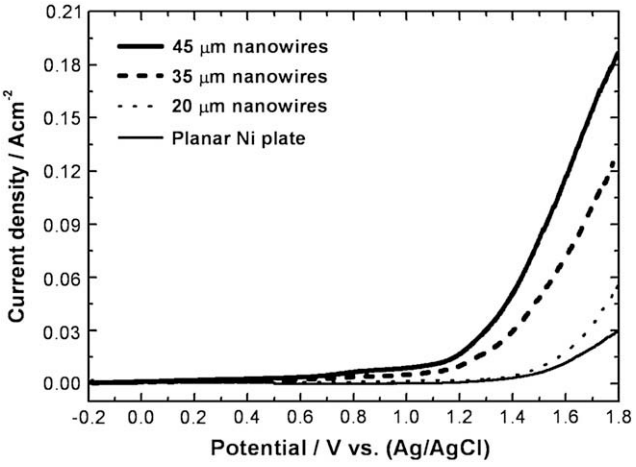

Fig. 7 – OER current–potential profiles for the Ni nanowires in exposed lengths of 20, 35, and 45 μm, as well as planar Ni plate.

After confirming enhancements in the HER for the Ni nanowires in transient measurements, it would be necessary to evaluate their galvanostatic behaviors for lifetime determination. Fig. 6 exhibits the voltage profiles for the supported (20 μm in exposed length) and unsupported (45 μm in exposed length) Ni nanowires. The supported and unsupported Ni nanowires revealed voltage plateau of −1.329 and −1.224 V, respectively. Accordingly, the overpotentials for the HER were 1.129 and 1.024 V. These values agreed well with earlier i–V curves, where longer exposed Ni nanowires resulted in better HER performances. Interestingly, the voltage profiles were reasonably flat, indicating that the electrode structures were not damaged after release of gas bubbles. Moreover, SEM images confirmed the samples were still in reasonable shape after 22 h. It is to be noted that during HER in neutral electrolyte, local formation of NaOH, and its accompanying pH change, is unlikely to affect the chemical stability of Ni.

The i–V polarizations for the OER are provided in Fig. 7. As shown, these samples revealed notable current outputs when the applied potentials became more anodic. For voltage below 0.8 V, the increases in the current densities were relatively subdued. At voltage above 0.8 V, they demonstrated significant current responses. In particular, the Ni nanowires with longer exposed lengths revealed larger current values, a fact consistent with that of HER. In contrast, the planar Ni plate

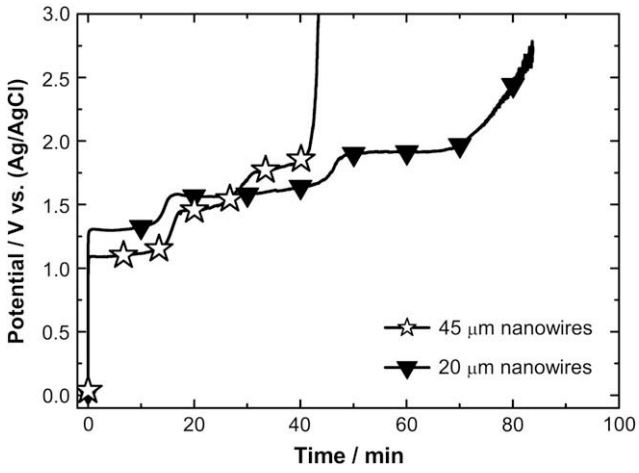

Fig. 8 – Galvanostatic OER profiles for the Ni nanowires in 20 (▼) and 45 (☆) μm, respectively.

exhibited substantially lower current densities even at anodic voltage above 1.5 V. It is noted that the recorded current responses during OER also include inevitable Ni oxidation. Hence, the exact OER currents were expected to be moderately reduced.

Fig. 8 exhibits the OER galvanostatic measurements for the Ni nanowires of exposed length of 20 (supported) and 45 (unsupported) μm. As shown, both samples demonstrated step-wise increases in the output voltages as time progressed. This phenomenon is due to the inherent Ni oxidation under anodic condition that results in higher OER overpotential [33]. In the first 10–15 min, the supported and unsupported Ni nanowires displayed voltage plateaus at 1.304 and 1.094 V, respectively. These values were close to what were measured in earlier OER i–V polarizations. However, the unsupported Ni nanowires suffered from substantial performance degradations with steady voltage increments. At 40 min, the unsupported sample failed and detached from the sample holder, resulting in a sharp rise in the voltage. In contrast, the supported Ni nanowires revealed a relatively slower degradation behavior despite its initial voltage was slightly higher than that of the unsupported one. The supported Ni nanowires sustained until 70 min before the breakdown took place. We understand that during OER, H_2SO_4 was formed locally. Therefore, stability of Ni nanowires was possibly affected by acidic attack. Since the supported Ni nanowires not only revealed less exposed area but also were surrounded by AAO pore walls, their improved mechanical robustness and better lifetime were not unexpected.

Our results so far establish that the Ni nanowires can be used for HER but not applicable to OER. Nevertheless, a preliminary determination on the hydrogen production energy cost using the Ni nanowires for both electrodes is still necessary. Basing on voltage reading from the galvanostatic HER and OER data, and assuming a 100% coulombic efficiency, we estimated the energy cost for hydrogen production as 5.65×10^5 J/mole and 5.24×10^5 J/mole for Ni nanowires in 20 and 45 μm length, respectively. In comparison, the thermodynamic value for hydrogen production from liquid water at 298 K is 2.86×10^5 J/mole. Unfortunately, the energy cost for hydrogen production using the Ni nanowires in a neutral electrolyte is significantly larger than what was reported recently by Merriall and Dougherty using metal oxides in an alkaline system [34]. However, we realize the hydrogen production energy cost for the Ni nanowires could be further reduced once an alkaline electrolyte in conjunction with elevated operation temperature is adopted. Because the overpotential from the OER during water electrolysis is recognized as the principal contributor for energy loss, considerable performance improvements are certainly likely when nanoparticles of known electrocatalysts ($NiCo_2O_4$, IrO_2) are impregnated on the Ni nanostructures to further reduce the OER overpotential [35,36].

4. Conclusions

Using a dc pulse electrodeposition technique, we prepared the Ni nanowires in lengths of 45 μm within the pore channels of AAO template. The diameter for the Ni nanowires was 250 nm, resulting in an aspect ratio of 180. After selective etching to remove the supporting pore walls, we fabricated free-standing, as well as supported Ni nanowires with exposed lengths of 35 and 20 μm. For HER in 1 M Na_2SO_4, both the i–V and galvanostatic measurements indicated that Ni nanowires with longer exposed lengths delivered better performances. However, the effective current density for the Ni nanowires was smaller than that of planar Ni plate. Values in double-layer capacitance from impedance spectra suggested electrolyte mass transport within the nanowires electrode might be accountable for the reduction in electrochemical active surface area. In i–V polarizations for OER, the Ni nanowires with longer exposed lengths revealed larger current outputs. However, in galvanostatic lifetime determinations, the supported Ni nanowires demonstrated a better lifetime. Estimation on the hydrogen production energy cost was also provided.

Acknowledgement

Financial support from the National Science Council of Taiwan under the contract of NSC96-2221-E-009-110 is greatly appreciated. Equipment loan from Professor Pang Lin is noted.

REFERENCES

[1] Steele BCH, Heinzel A. Materials for fuel-cell technologies. Nature 2001;414:345–52.
[2] Rashkov R, Arnaudova M, Avdeev G, Zielonka A, Jannakoudakis P, Jannakoudakis A, et al. NiW/TiO_x composite layers as cathode material for hydrogen evolution reaction. Int J Hydrogen Energy 2009;34:2095–100.
[3] Stojić DL, Marčeta MP, Sovilj SP, Miljanić SS. Hydrogen generation from water electrolysis – possibilities of energy saving. J Power Sources 2003;118:315–9.

[4] Suffredini HB, Cerne JL, Crnkovic FC, Machado SAS, Avaca LA. Recent developments in electrode materials for water electrolysis. Int J Hydrogen Energy 2000;25:415–23.
[5] Marshall AT, Sunde S, Tsypkin M, Tunold R. Performance of a PEM water electrolysis cell using $Ir_xRu_yTa_zO_2$ electrocatalysts for the oxygen evolution electrode. Int J Hydrogen Energy 2007;32:2320–4.
[6] Stojić DL, Grozdić TD, Kaninski MPM, Stanić VĐ. Electrocatalytic effects of Mo–Pt intermetallics singly and with ionic activators. Hydrogen production via electrolysis. Int J Hydrogen Energy 2007;32:2314–9.
[7] Han Q, Liu K, Chen J, Wei X. Preparation of the composite $LaNi_{3.7}Al_{1.3}$/Ni–S–Co alloy film and its HER activity in alkaline medium. Int J Hydrogen Energy 2009;34:71–6.
[8] Xu Y. The hydrogen evolution reaction on single crystal gold electrode. Int J Hydrogen Energy 2009;34:77–83.
[9] Kibria MF, Mridha MS. Electrochemical studies of the nickel electrode for the oxygen evolution reaction. Int J Hydrogen Energy 1996;21:179–82.
[10] Kellenberger A, Vaszilcsin N, Brandl W, Duteanu N. Kinetics of hydrogen evolution reaction on skeleton nickel and nickel–titanium electrodes obtained by thermal arc spraying technique. Int J Hydrogen Energy 2007;32:3258–65.
[11] Kim DR, Cho KW, Choi YI, Park CJ. Fabrication of porous Co–Ni–P catalysts by electrodeposition and their catalytic characteristics for the generation of hydrogen from an alkaline $NaBH_4$ solution. Int J Hydrogen Energy 2009;34:2622–30.
[12] Lu G, Evans P, Zangari G. Electrocatalytic properties of Ni-based alloys toward hydrogen evolution reaction in acid media. J Electrochem Soc 2003;150:A551–7.
[13] Kaninski MPM, Nikolic VM, Tasic GS, Rakocevic ZL. Electrocatalytic activation of Ni electrode for hydrogen production by electrodeposition of Co and V species. Int J Hydrogen Energy 2009;34:703–9.
[14] Lupi C, Dell'Era A, Pasquali M. Nickel–cobalt electrodeposited alloys for hydrogen evolution in alkaline media. Int J Hydrogen Energy 2009;34:2101–6.
[15] Nylén L, Behm M, Cornell A, Lindbergh G. Investigation of the oxygen evolving electrode in pH-neutral electrolytes-modelling and experiments of the RDE-cell. Electrochim Acta 2007;52:4513–24.
[16] Grosjean MH, Zidoune M, Roué L, Huot JY. Hydrogen production via hydrolysis reaction from ball-milled Mg-based materials. Int J Hydrogen Energy 2006;31:109–19.
[17] Izumida T, Kato K, Kawamura F, Yusa H. Electrolytic decontamination of surface-contaminated metal by alternating electrolysis using square-wave current in a neutral salt electrolyte. Nucl Technol 1985;70:249–53.
[18] Bao J, Tie C, Xu Z, Zhou Q, Shen D, Ma Q. Template synthesis of an array of nickel nanotubules and its magnetic behavior. Adv Mater 2001;13:1631–3.
[19] Chen PL, Huang WJ, Chang JK, Kuo CT, Pan FM. Fabrication and field emission characteristics of highly ordered titanium oxide nanodot arrays. Electrochem Solid State Lett 2005;8:H83–6.
[20] Sides CR, Martin CR. Nanostructured electrodes and the low-temperature performance of Li-ion batteries. Adv Mater 2005;17:125–8.
[21] Li N, Mitchell DT, Lee KP, Martin CR. A nanostructured honeycomb carbon anode. J Electrochem Soc 2003;150:A979–84.
[22] Sapp SA, Lakshmi BB, Martin CR. Template synthesis of bismuth telluride nanowires. Adv Mater 1999;11:402–4.
[23] Song GJ, Chen D, Peng Z, She X, Li J, Han P. Quantificational etching of AAO template. J Mater Sci Technol 2007;23:427–9.
[24] Burdick J, Alonas E, Huang HC, Rege K, Wang J. High-throughput templated multisegment synthesis of gold nanowires and nanorods. Nanotechnology 2009;20:1–6.
[25] Liu XM, Zhou VC. Electrochemical deposition and characterization of Cu_2O nanowires. Appl Phys A 2005;81:685–9.
[26] Kiuchi D, Matsushima H, Fukunaka Y, Kuribayashi K. Ohmic resistance measurement of bubble froth layer in water electrolysis under microgravity. J Electrochem Soc 2006;153:E138–43.
[27] Cheng H, Scott K, Ramshaw C. Intensification of water electrolysis in a centrifugal field. J Electrochem Soc 2002;149:D172–7.
[28] Kim S, Koratkar N, Karabacak T, Lu TM. Water electrolysis activated by Ru nanorod array electrodes. Appl Phys Lett 2006;88:263106–9.
[29] Michishita H, Misumi Y, Haruta D, Masaki T, Yamamoto N, Matsumoto H, et al. Cathodic performance of $La_{0.6}Sr_{0.4}CoO_3$ perovskite oxide for platinum-free alkaline water electrolysis cell. J Electrochem Soc 2008;155:B969–71.
[30] Vázquez-Gómez L, Cattarin S, Guerriero P, Musiani M. Hydrogen evolution on porous Ni cathodes modified by spontaneous deposition of Ru or Ir. Electrochim Acta 2008;53:8310–8.
[31] Orazem ME, Pébère N, Tribollet B. Enhanced graphical representation of electrochemical impedance data. J Electrochem Soc 2006;153:B129–36.
[32] Brug GJ, Van Den Eeden ALG, Sluyters-Rebach M, Sluyters JH. The analysis of electrode impedances complicated by the presence of a constant phase element. J Electroanal Chem 1984;176:275–95.
[33] Medway SL, Lucas CA, Kowal A, Nichols RJ, Johnson D. In situ studies of the oxidation of nickel electrodes in alkaline solution. J Electroanal Chem 2006;587:172–81.
[34] Merrill MD, Dougherty RC. Metal oxide catalysts for the evolution of O_2 from H_2O. J Phys Chem C 2008;112:3655–66.
[35] Bocca C, Barbucci A, Delucchi M, Cerisola G. Nickel–cobalt oxide-coated electrodes: influence of the preparation technique on oxygen evolution reaction (OER) in an alkaline solution. Int J Hydrogen Energy 1999;24:21–6.
[36] Rasten E, Hagen G, Tunold R. Electrocatalysis in water electrolysis with solid polymer electrolyte. Electrochim Acta 2003;48:3945–52.